Journal of Magnetism and Magnetic Materials 360 (2014) 52–58

Contents lists available at ScienceDirect

Journal of Magnetism and Magnetic Materials

journal homepage: www.elsevier.com/locate/jmmm

Measurement of the magnetic properties of P9 and T22 steel taken from service in power station

J.W. Wilson [a,*], N. Karimian [a], J. Liu [b], W. Yin [a], C.L. Davis [b], A.J. Peyton [a]

[a] School of Electrical and Electronic Engineering, University of Manchester, Manchester M13 9PL, UK
[b] School of Metallurgy and Materials, University of Birmingham, Edgbaston, Birmingham B15 2TT, UK

ARTICLE INFO

Article history:
Received 24 October 2013
Received in revised form
17 January 2014
Available online 31 January 2014

Keywords:
NDE
Electromagnetic
Barkhausen
Steel
Permeability
Hysteresis

ABSTRACT

With the UK's aging power generation network, life-extension of steel plant components is a critical issue. However, in order to evaluate the likelihood of component failure, techniques must be developed to properly assess the level of degradation in power station steels. Electromagnetic inspection has the potential to quantify the level of degradation through in-situ measurements at elevated temperatures. This paper reports the results of tests carried out on thermally treated P9 and T22 steel samples with different microstructural states using major and minor *B–H* loop measurements and magnetic Barkhausen noise measurements. The results show that by careful selection of minor loop parameters, specific to the material under inspection and the material change under consideration, correlations can established between EM properties and material properties such as Vickers hardness. These results will be used as a basis for the further development of a fully field deployable device.

1. Introduction

Current procedures for the assessment of the condition of components in power stations involve site inspections during costly shutdown periods and inspection of steel components often involves lengthy procedures such as replica metallography [1,2] or hardness testing. The use of electromagnetic (EM) sensors for inspection has the potential to provide information on microstructural changes in steel by exploiting the link between the microstructure and magnetic domain structure of the material. EM inspection [3–5] has the advantage that it can be performed in-situ, at elevated temperatures, with minimal surface preparation.

A number of different approaches are available to assess the magnetic properties of a particular material, the most basic of these is the calculation of the major *BH* loop. Values derived from the major loop, such as coercivity, permeability and hysteresis loss, can be used to quantify the magnetic hardness of a material, which in turn is indicative of material hardness [6]. In addition to these major loop properties, information can also be derived from small minor loop deviations from the major loop or initial magnetisation curve.

Although these two techniques both involve the measurement of magnetic flux density *B* in response to an applied field *H*, the interaction between magnetic domains and material microstructure can be different. The major loop response consists of a combination of reversible and irreversible components [7]; irreversible magnetisation from domain walls overcoming pinning sites such as inclusions, dislocations and grain boundaries and reversible magnetisation from domain wall motion and rotation of magnetic domains. In contrast, the minor loop response to a small applied field is predominantly reversible; corresponding to bowing of domain walls and domain rotation at higher major loop offsets [7].

Previous work has highlighted the strengths of minor loop measurement for the assessment of material degradation. For example Takahashi et al. [8] carried out minor loop measurements on low carbon steel exposed to differing levels of cold rolling. The steel was machined into picture frame samples and wound with exciting and detecting coils. Various parameters were extracted from the minor loops, including minor loop coercivity, remanence and susceptibility. These minor loop parameters were shown to have a strong correlation to Vickers hardness and DBTT, whereas major loop coercivity was shown to increase in proportion to the square root of dislocation density.

The link between magnetic Barkhausen noise (MBN) activity and material properties such as hardness [9] and residual stress is more complex, but by using techniques such as analysis of the MBN profile, a more comprehensive understanding of the magnetic domain structure of the material can be developed. Through this deeper understanding of the domain structure, information pertaining to the material microstructure can be inferred through the interaction between domain walls and microstructural features such as dislocations, grain boundaries and precipitates. As these

* Corresponding author. Tel.: +44 161 306 8716.
E-mail addresses: John.Wilson@manchester.ac.uk, john.w.wilson999@gmail.com (J.W. Wilson).

0304-8853/$ - see front matter © 2014 Elsevier B.V. All rights reserved.
http://dx.doi.org/10.1016/j.jmmm.2014.01.057

microstructural changes e.g. the coarsening of martensitic laths and precipitates are major causes of failure for power station steels, MBN could be a useful tool for the quantification of degradation, when used in conjunction with other techniques [10–13].

Although major *B*–*H* loop features are useful, this type of measurement is difficult to achieve on open samples (i.e. pipes and tubes). MBN and permeability readings derived from minor loops are easier on open samples, require less power, and by looking at the change in readings rather than absolute values, may not require an accurate *H* field measurement; as accurate *H* measurement is to some extent dependent on geometry. By utilising a number of minor loop measurement techniques, material specific correlations can be established between microstructural changes of interest and selected minor loop features [14,15].

In this paper, the results of tests carried out on EM characterisation of power station steels are provided. Section 2 details the equipment constructed for the tests and gives an overview of the steel samples. The experimental results are provided in Section 3, including; magnetic Barkhausen noise (MBN) with major *B*–*H* loop excitation; the derivation of incremental permeability curves using minor *B*–*H* loop excitation and MBN measurement with minor loop excitation. The paper concludes with discussion and conclusion sections where the test results are compared to Vickers hardness values and the possibility of employing the techniques on open tube samples is discussed.

2. Measurement system and sample summary

2.1. Measurement system

A schematic of the measurement system developed for the tests is shown in Fig. 1. A low frequency time varying signal is fed to two power amplifiers, which supply current to two excitation coils wrapped around a silicon-steel core. The cylindrical sample to be tested is fitted into a slot in the core, to maximise coupling between core and sample. The axial applied field (*H*) is measured using a Quantum Well Hall sensor, developed at the University of Manchester. The GaAs–InGaAs–AlGaAs Hall Sensor has a sensitivity of 0.16 mV/mA mT, and is capable of detecting magnetic fields as low as 10 nT and as high as 10 s of Tesla [16]. The flux density of the induced field (*B*) is measured using a 20-turn encircling coil connected to an instrumentation amplifier. For MBN measurements, the 20-turn coil is replaced with a 6000-turn encircling coil and the low frequency component of the signal is rejected through the addition of a passive 5 kHz high-pass filter.

For the major loops, a 1 Hz sinusoidal excitation is used and 9 cycles are recorded and averaged. A 10 Hz sinusoidal excitation is used to generate the minor loops, with two types of minor loop being recorded; (1) deviations from the main *B*–*H* loop. In this case, the sample is taken through several major loop cycles before the applied field is held constant at a pre-determined *H* value and several minor loop cycles are recorded; (2) deviations from the initial magnetisation curve. The sample is demagnetised by the application of 10 Hz sinusoidal excitation, gradually reducing in amplitude. The applied field is then increased to a pre-determined *H* value and several minor loop cycles recorded. For both types of minor loop, up to 90 cycles are acquired and averaged, to reduce noise.

The 1 Hz sinusoidal excitation is used to generate major loop MBN profiles, with the signal from the MBN pickup coil and the applied axial field from the Hall sensor being recorded simultaneously. The signal from the coil is then high-pass filtered at a frequency of 5 kHz, rectified, and a moving average technique used to generate the MBN profile, which is then plotted against *H*. A similar process is used for the minor loop MBN readings, with the minor loop generated as outlined above.

2.2. Test samples

Two sample sets have been studied, consisting of three P9 and three T22 steel samples. Both steels were taken from components removed from service for approximately eleven years at 520 °C. Selected samples (approx. 70 mm × 15 mm × 7 mm) were heat treated to simulate service entry microstructure i.e. tempered martensite/bainite, by normalising at 950 °C for 1 h or 940 °C for

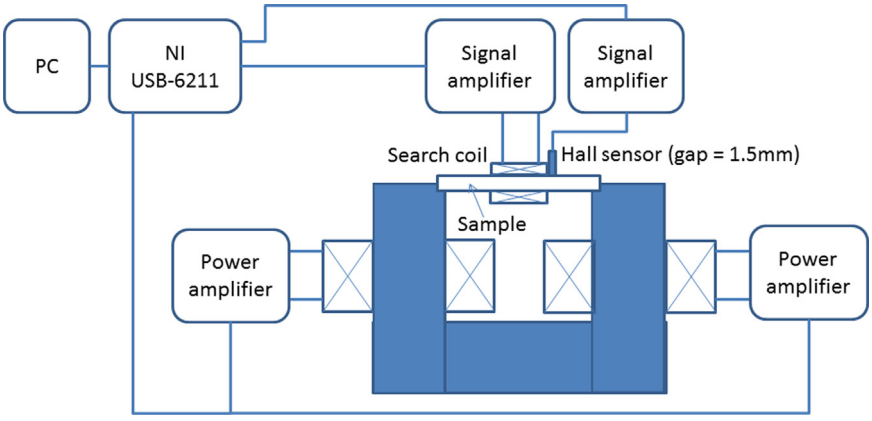

Fig. 1. Schematic of measurement apparatus.

Table 1
Sample composition (in wt%) and heat treatments.

	P9					T22				
	Cr	**Mo**	**C**	**Si**	**Mn**	**Cr**	**Mo**	**C**	**Si**	**Mn**
%	8.4	0.97	0.12	0.52	0.44	2.14	1.01	0.15	0.28	0.44
	P9-TEMP		**P9-TFS**	**P9-NORM**		**T22-TEMP**		**T22-TFS**	**T22-NORM**	
	Tempered at 760 °C for 1 h		Taken from service	Normalised at 950 °C for 1 h		Tempered at 760 °C for 1 h		Taken from service	Normalised at 950 °C for 1 h	

1 h followed by air cooling to room temperature and then tempering at 760 °C for 1 h or 720 °C for 1.5 h for P9 and T22, respectively. The as-normalised samples were also assessed. The heat treatment conditions have been determined as per ASTM standards A335 [17] and A213 [18] as well as literature data [19–22]. Heat treatments, composition details and Vickers Hardness numbers (HV) are given in Table 1. Cylindrical rods with a diameter of 4.92 ± 0.03 mm and a length of 49.59 ± 0.54 mm were machined from each of the samples.

Complete metallographic tests were carried out for each heat treatment condition; micrographs for the tests have been presented previously [3,4]. The microstructure of the as-normalised P9 consists of predominantly martensite mixed with some bainite, which gives a high hardness value (HV 401). Subsequent tempering produces a simulated service entry microstructure, i.e. tempered martensite/bainite, with a significant drop in hardness to HV 212. After long service exposure, the microstructure showed equiaxed ferrite with large carbides distributed within ferrite grains or on grain boundaries, with a further decrease in hardness to HV 158.

The as-normalised T22 steel shows a mixed microstructure of bainite and some pro-eutectoid ferrite. No carbides are present in the ferrite, but plate-like carbides can be seen within the bainite region. After tempering, many carbides can be observed along prior austenite grain boundaries, on ferrite boundaries or within bainite regions. The microstructure of T22 after service exposure consists of equiaxed ferrite and a great many carbides outlining the ferrite grain boundaries or finely dispersed within the ferrite grains. The HV values follow the same trend as the P9 samples, with a high hardness value (HV 316) for the as-normalised sample, and a significant drop to HV 203 and HV 128 after the tempering and the long service exposure, respectively.

3. Measurement and experimental results

3.1. Major B–H loop and MBN measurements

Fig. 2 shows major B–H loops for both sample sets. Examination of the coercivity (H_C) values (see Table 2) in comparison to the hardness values shows that H_C increases with increasing hardness, though the decrease in H_C for service exposure is relatively small. Fig. 3 shows the MBN profiles plotted with the corresponding section of the BH loop. It is apparent from the plots that although the MBN profile peaks do not exactly correspond to the coercive force, they do follow the trend in H_C, with the peak for P9-TFS at the lowest H value and the peak for P9-NORM at the highest H value. Thus, the MBN peak position is indicative of the hardness of the P9 samples. The MBN profile for P9-NORM is of the form generally expected for martensitic materials, a broader peak at a higher applied field [10]. This is due to the domain walls overcoming the pinning from a high density of martensitic lath/block/packet boundaries and dislocation networks. Subsequent tempering produces a tempered martensite/bainite structure, resulting in a higher MBN peak amplitude at a much lower applied field. This is consistent with previous studies [10,23], where the recovery of the highly strained martensite and the coarsening of the martensitic/bainitic laths and the precipitates due to the tempering result in higher amplitude low H field peaks. The MBN profile for P9-TFS demonstrates the effect of long service exposure at high temperatures. The MBN peak position has shifted to a lower H field as the material has softened in service.

The MBN profiles for the T22 samples broadly follow the same trends as those for the P9 samples, with one obvious exception; the major peak for the tempered sample corresponds to a lower H field than that for the ex-service sample. There is however a second peak in the profile for T22-TEMP at a higher H field; one interpretation of this is that the low field peak corresponds to overcoming pinning from the grain/lath boundaries and the higher field peak (Peak 2, Fig. 3b) corresponds to the carbide precipitates [13].

3.2. Minor loop measurements

The evolution of the minor loop as deviations from the initial magnetisation curve is shown in Fig. 4. The origin of the first minor loop corresponds to the demagnetised state ($B=0$, $H=0$). In this state, for a small applied field (H), the magnetisation (M) of the material can be described by Raleigh Law [24]:

$$M = \chi_0 H + \alpha_R \mu_0 H^2 \quad (1)$$

Table 2
Major loop, permeability and MBN values.

	P9-TEMP	P9-TFS	P9-NORM	T22-TEMP	T22-TFS	T22-NORM
HV	212	158	401	203	129	316
***BH* loop**						
MBN$_{PK}$ (mV_{rms})	2.33	1.61	0.23	2.06	0.95	0.37
MBN$_{POS}$ (kA/m)	0.50	0.29	3.35	0.68 (pk. 2)	0.41	1.87
***H*$_C$ (kA/m)**	0.70	0.43	3.43	0.66	0.59	1.99
Minor loop						
μ_{IC}	89.8	135.9	35.0	84.2	85.2	60.8
μ_{BH}	78.8	139.7	37.0	70.3	89.4	59.4
μ_i	90.2	120.4	31.7	66.6	95.3	53.3
MBN$_{\mu i}$ (mV_{rms})	0.46	1.03	0.18	0.31	0.46	0.19

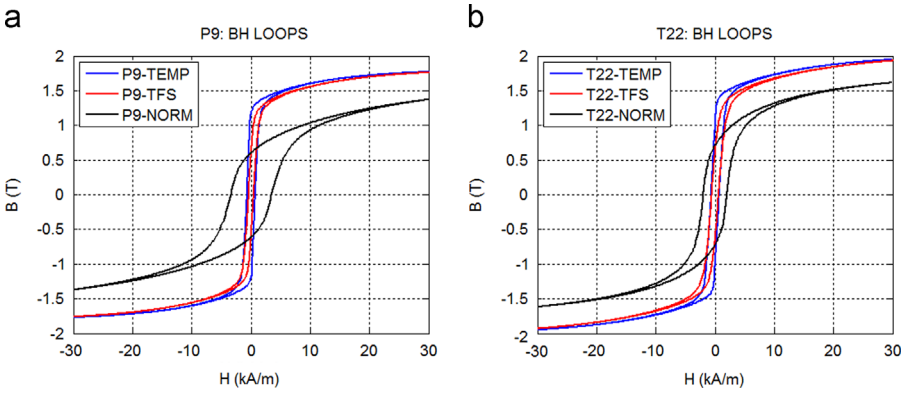

Fig. 2. *BH* loops for (a) P9 samples, (b) T22 samples.

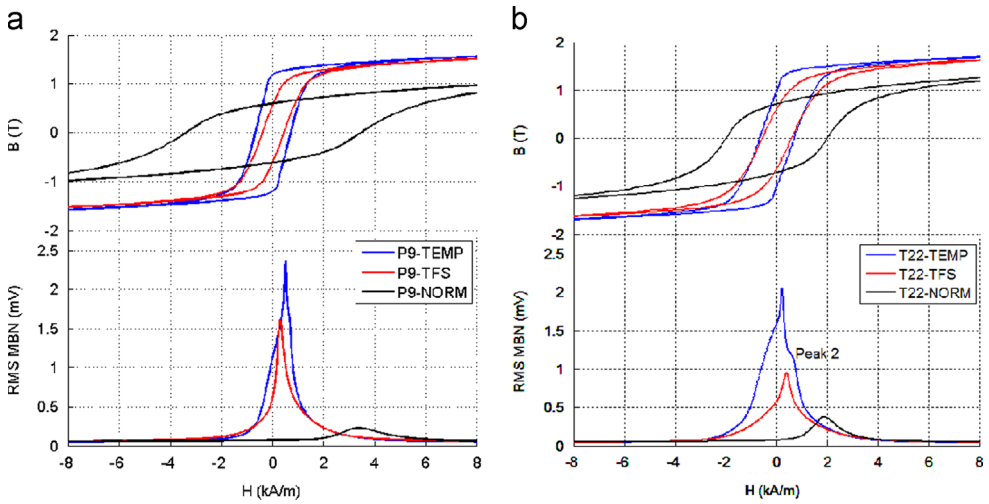

Fig. 3. *B–H* loops and corresponding MBN profiles for (a) P9 samples, (b) T22 samples.

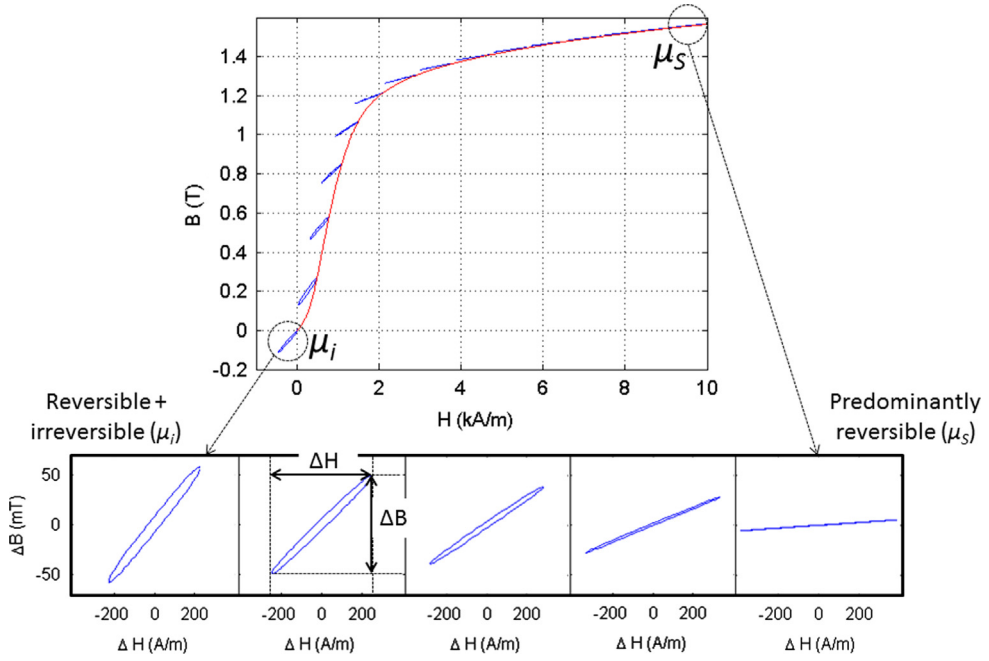

Fig. 4. Initial magnetisation curves and minor loop deviations for P9-Temp (*B* and *H* offsets removed from minor loops for comparison).

where χ_0 is initial susceptibility, describing the reversible part of magnetisation, the Rayleigh constant α_R describes the irreversible Barkhausen jumps and μ_0 is the permeability of free space. Thus, in this region, magnetisation is a combination of reversible and irreversible components, resulting in a loop enclosing a relatively large area, as show in Fig. 4 (bottom left). As the initial magnetisation curve approaches saturation, domain walls are swept away by field pressure and the dominant magnetisation mechanism is the progressive alignment of the domains with the applied field direction [24]. Thus, reversible components become dominant, resulting in a loop with a much smaller area, with a smaller ΔB for a given ΔH, as shown in Fig. 4 (bottom right).

Incremental permeability (μ_Δ) is calculated as the ratio between the change in flux density (ΔB) and the change in the applied field (ΔH) scaled with respect to the permeability of free space (μ_0)

$$\mu_\Delta = \Delta B/(\Delta H \times \mu_0).$$

Fig. 5a–c shows the three types of minor loop configurations used to derive incremental permeability values; minor loop deviations from the initial magnetisation curve (Fig. 5a) and major *BH* loop (Fig. 5b) and a minor loop amplitude sweep (Fig. 5c). The incremental permeability values for the three minor loop configurations are shown in Fig. 5d–f, respectively.

Fig. 5d shows the resultant incremental permeability curves for minor loop deviations from the initial magnetisation curve. It can be seen from the plot that the maximum values (μ_{IC}) correspond to the origin of the initial magnetisation curve, i.e. the point at which domains have the greatest degree of freedom to move, resulting in the greatest change in *B* for a given applied field. There is a sharp decrease in μ_Δ with increasing *H* and some convergence in μ_Δ values for the three samples from each material (P9 and T22) as saturation is approached and contributions from domain wall pinning sites are reduced, giving way to reversible domain rotation effects. P9-NORM exhibits a much smaller variation in μ_Δ for increasing *H*, as the high dislocation density of the predominantly

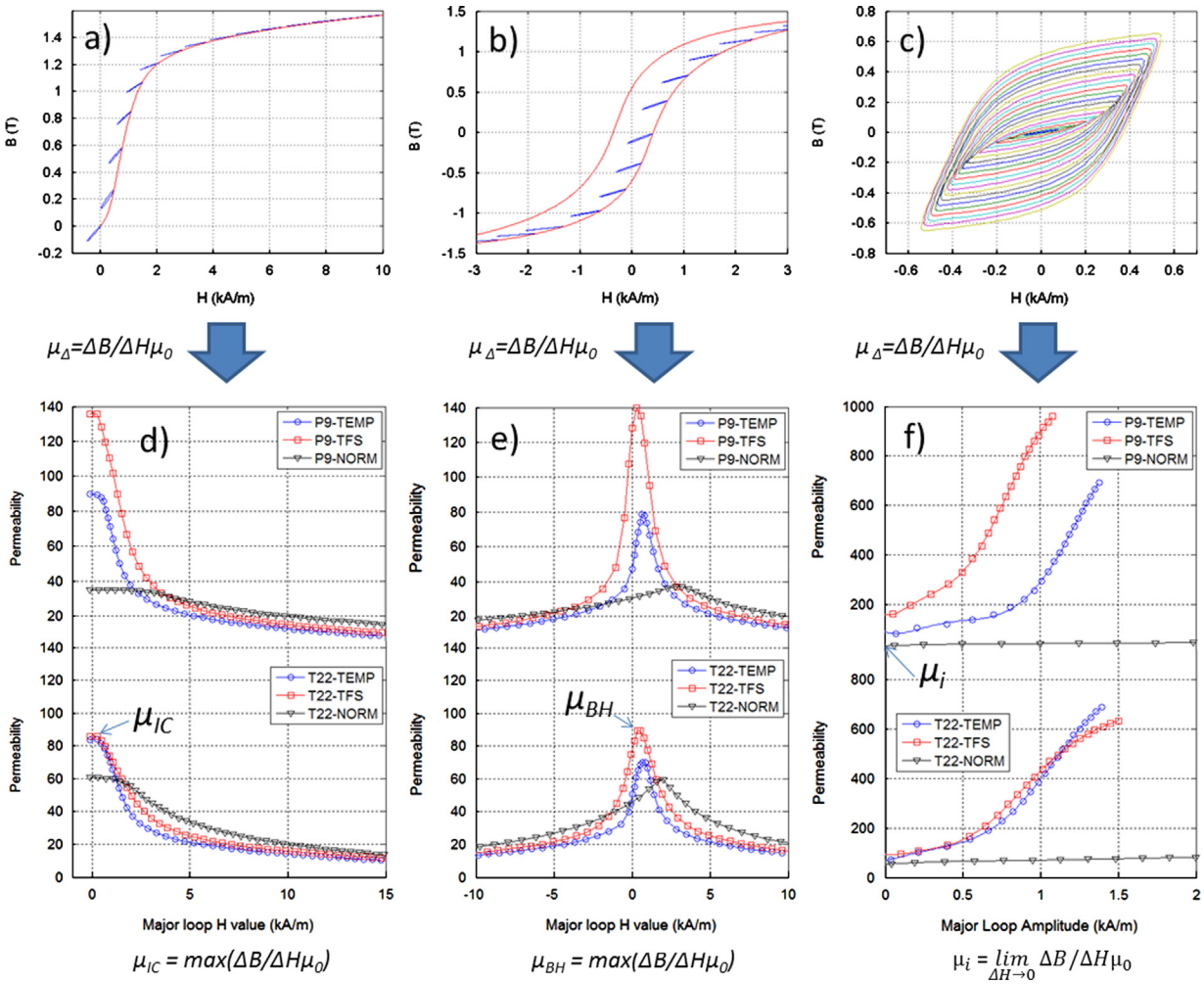

Fig. 5. Derivation of incremental permeability (μ_Δ) curves from minor loops; (a) minor loop deviations from initial magnetisation curve, (b) minor loop deviations from *BH* loop, (c) minor loop amplitude sweep, (d) incremental permeability values derived from initial magnetisation curve, (e) incremental permeability values derived from *BH* loop, (f) incremental permeability values derived from minor loop amplitude sweep.

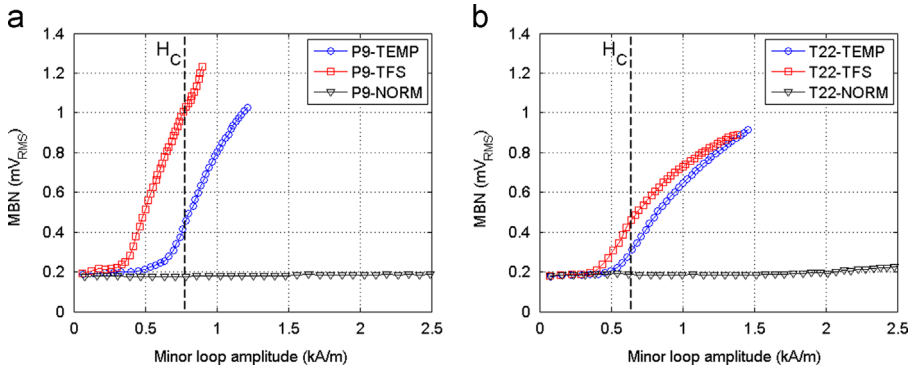

Fig. 6. MBN_{RMS} values derived from initial permeability (μ_i) minor loop amplitude sweep for; (a) P9 sample set (b) T22 sample set.

martensitic sample results in heavy domain wall pinning and irreversible magnetisation effects are minimised.

Fig. 5e shows the μ_Δ curves for minor loop deviations from the major *B*–*H* loop. It can be seen from the plot that the maximum μ_Δ value (μ_{BH}, Table 2) occurs close to the coercive force, which is in agreement with literature [25]. As with the initial curve results, this is the point at which $B=0$ and domain walls have the greatest degree of freedom to move.

Fig. 5f shows plots of μ_Δ for P9 and T22 for a variation in minor loop amplitude. It can be seen from the plots that as the minor loop amplitude increases, so does μ_Δ. At low minor loop amplitudes, reversible magnetisation dominates ($\chi_0 H$, Eq. (1)) as the minor loop amplitude increases, the irreversible component ($(\alpha_R\mu_0 H^2$ Eq. (1)) is introduced and the gradient of the minor loop increases, as a greater ΔB is generated for a given change in *H*. Polynomial fitting has been employed to extrapolate values for

μ_Δ if the minor loop amplitude could be made to equal zero; see μ_i, Table 2.

3.3. Minor loop magnetic Barkhausen noise

The change in MBN_{RMS} values derived from a minor loop amplitude sweep (see Fig. 5c) for initial permeability is shown in Fig. 6a. It can be seen from the plot that at higher minor loop amplitudes, MBN_{RMS} follows a similar trend to the permeability values derived from the minor loop amplitude sweep, as shown in Fig. 5f; with the MBN value for the P9 ex-service sample increasing rapidly and reaching the highest amplitude, increasing less rapidly for the tempered sample and exhibiting very little change for the normalised sample. However, at lower amplitudes the plots for the three samples converge, only showing a significant increase in amplitude at around 0.3 kA/m for P9-TFS and 0.5 kA/m for P9-TEMP. This indicates that only at these higher applied fields do the domain walls gain enough energy to overcome particular pinning sites in the material.

The plots for the T22 samples (Fig. 6b) exhibit a similar trend. However in contrast with the results for P9, T22-TFS and T22-TEMP start to cross over, reflecting the fact that tempered samples give the highest level of MBN for major loop excitation (see Fig. 2). It is also notable that the point at which the samples exhibit a significant increase in amplitude is indicative of the trend in H_C.

In order to provide a single minor loop MBN reading for each sample ($MBN_{\mu i}$, Table 2), it was decided to choose the readings at the point where the minor loop amplitude reaches the coercivity value for P9-TEMP and T22-TEMP for the P9 and T22 sample sets, respectively. This point was chosen because the tempered samples represent the service entry microstructure of the two steels, therefore the H_C values represent a fundamental magnetic property of these steels.

4. Discussion

Table 2 shows the various signal features collected from the tests in this paper. All the minor loop features (μ_{IC}, μ_{BH}, μ_i, $MBN_{\mu i}$) have an inverse relationship with HV, increasing from normalised to tempered to taken-from-service. Although H_C is not proportional to HV, it does follow the same trend.

Fig. 7 shows selected features plotted with respect to hardness. The first two points on the plots correspond to the taken-from-service (TFS) and tempered (TEMP) samples, respectively; it is the change between these two points that is of greatest interest in the assessment of degradation in power station steels. Fig. 7a and b show the major loop features, coercivity (H_C) and MBN peak position (MBN_{POS}) plotted with respect to hardness. It can be seen from the plots that the change in the MBN_{POS} follows the change in H_C, as is shown in Fig. 3, although the change in H_C is comparatively small for the T22 samples. Previous work [8] has shown H_C to increase in proportion to the square root of dislocation density; it may be that the greater increase in H_C for the normalised samples (the third data point) is due to this phenomena.

Fig. 7c and d shows the minor loop features, plotted with respect to hardness. It can be seen from the plots that $MBN_{\mu i}$ exhibits the greatest change with the increase in hardness. From the minor loop features, μ_{BH} and μ_i offer the best correlation with hardness, with the value extracted from the initial magnetisation curve (μ_{IC}) performing quite poorly for T22. It is clear from Fig. 5f that the differences in permeability values in this region (i.e. around $H=0$, $B=0$) are very sensitive to loop amplitude, so careful selection of loop amplitude may yield better results for μ_{IC}. The results are in broad agreement with previous work [8], though it should be noted that the minor loop parameters studied in the referenced paper deliver a change in the opposite polarity to those

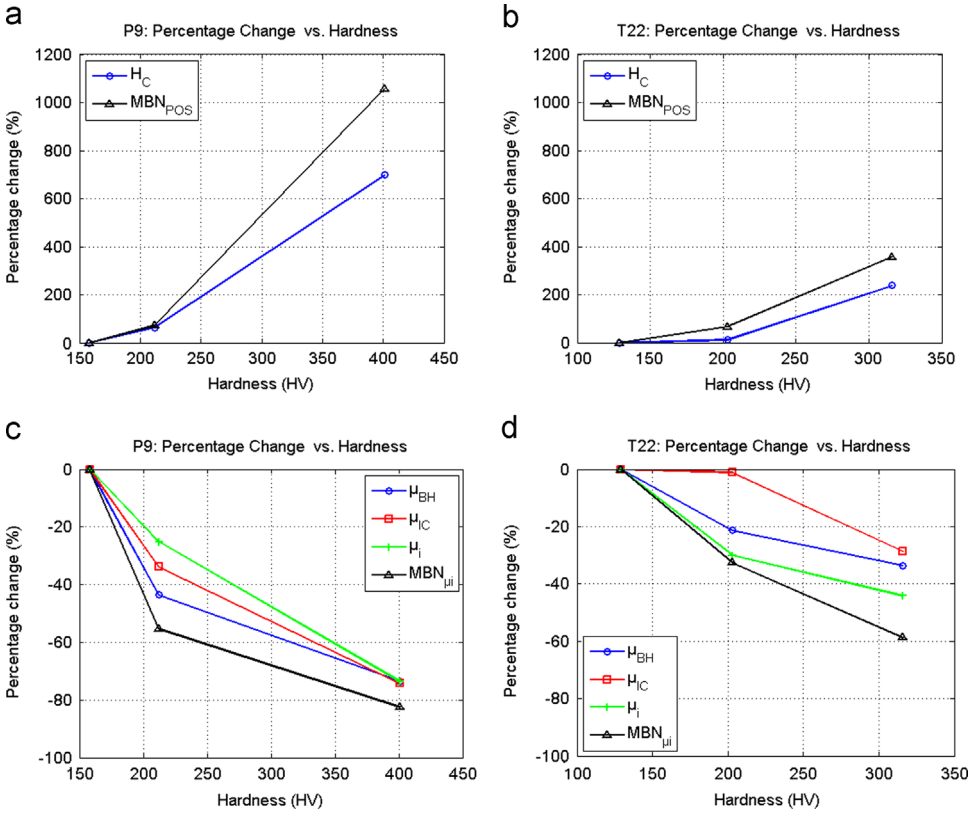

Fig. 7. Percentage change in *BH* loop features (H_C, MBN_{POS}) with respect to Vickers hardness for; (a) P9 sample set (b) T22 sample set. Percentage change in minor loop features ($\mu_{i\text{-}H0}$, $\mu_{\Delta\text{-}max}$, $MBN_{\mu i}$) with respect to Vickers hardness for; (c) P9 sample set (d) T22 sample set.

studied here, i.e. coercivity tends to increase with increasing magnetic hardness, whereas permeability tends to decrease.

5. Conclusions

This work shows that there are clear relationships between minor loop features and microstructural changes in power station steels. Correlations are material specific, thus careful selection of minor loop parameters for a given application is required. The next step of this work will be to exploit the correlations established using closed magnetic loop tests to develop a tool for the inspection of pipes and tubes in power stations. Provisional work [26] by the authors of this paper has demonstrated the applicability of these techniques to open samples, employing a coil encircling sections of Grade 91 power station tubing, used in conjunction with a magnetising yoke.

Acknowledgements

The authors greatly acknowledge the financial support of The Engineering and Physical Sciences Research Council (EPSRC) for this project under contract EP//H022937.

References

[1] C. Maharaj, J.P. Dear, A. Morris, A review of methods to estimate creep damage in low-alloy steel power station steam pipes, Strain 45 (4) (2009) 316–331.
[2] G. Sposito, C. Ward, P. Cawley, P.B. Nagy, C. Scruby, A review of non-destructive techniques for the detection of creep damage in power plant steels, NDT & E Int 43 (7) (2010) 555–567.
[3] J. Liu, X.J. Hao, L. Zhou, M. Strangwood, C.L. Davis, A.J. Peyton, Measurement of microstructure changes in 9Cr–1Mo and 2.25Cr–1Mo steels using an electromagnetic sensor, Scr. Mater. 66 (2012) 367–370.
[4] W. Yin, N. Karimian, J. Liu, X.J. Hao, L. Zhou, A.J. Peyton, M. Strangwood, C.L. Davis, Measurement of electromagnetic properties of power station steels, NDT & E Int 51 (2012) 135–141.
[5] J.W. Wilson, G.Y. Tian, V. Moorthy, B.A. Shaw, Magneto-acoustic emission and magnetic Barkhausen emission for case depth measurement in En36 gear steel, IEEE Trans. Magn 45 (2009) 177–183.
[6] H. Kumar, J.N. Mohapatra, R.K. RoyR. Justin JoseyphusA. Mitra, Evaluation of tempering behaviour in modified 9Cr–1Mo steel by magnetic non-destructive techniques, J. Mater. Process. Technol. 210 (4) (2010) 669–674.
[7] A. Hernando, P. Crespo, P. Marin, A. Gonzalez, Encyclopedia of materials: science and technology, Magn. Hysteresis (2001) 4780–4787.
[8] S. Takahashi, S. Kobayashi, H. Kikuchi, Y. Kamada, Relationship between mechanical and magnetic properties in cold rolled low carbon steel, J. Appl. Phys 100 (11) (2006) 113908–113908-6.
[9] L. Piotrowski, B. Augustyniak, M. Chmielewski, J. Labanowski, M. Lech-Grega, Study on the applicability of the measurements of magnetoelastic properties for a nondestructive evaluation of thermally induced microstructure changes in the P91 grade steel, NDT & E Int. 47 (2012) 157–162.
[10] O. Saquet, Barkhausen noise from plain carbon steels: analysis of the influence of microstructure, Mater. Sci. Eng., A 269 (1999) 73–82.
[11] J.A. Pérez-Benítez, J.H. Espina-Hernández, P. Martínez-Ortiz, A.F. Chávez-González, J.M. de la Rosa, Analysis of the influence of some magnetizing parameters on magnetic Barkhausen noise using a microscopic model, J. Magn. Magn. Mater. 347 (2013) 51–60.
[12] J.N. Mohapatra, N.R. Bandyopadhyay, M.K. Gunjan, A. Mitra, Study of high-temperature ageing and creep on bainitic 5Cr–0.5Mo steel by magnetic NDE techniques, J. Magn. Magn. Mater. 322 (6) (2010) 589–595.
[13] V. Moorthy, S. Vaidyanathan, Baldev Raj, T. Jayakumar, B.P. Kashyap, Insight into the microstructural characterization of ferritic steels using micromagnetic parameters, Metall. Mater. Trans. A 31 (4) (2000) 1053–1065.
[14] G. Vértesy, I. Tomáš, Complex characterization of degradation of ferromagnetic materials by magnetic adaptive testing, IEEE Trans. Magn. 49 (6) (2013) 2881–2885.
[15] G. Dobmann, I. Altpeter, B. Wolter, R. Kern, Industrial applications of 3MA–micromagnetic multiparameter microstructure and stress analysis, Electromagn. Nondestr. Eval. (XI) 31 (2008) 18–25.
[16] N. Haned, M. Missous, Nano-tesla magnetic field magnetometry using an InGaAs–AlGaAs–GaAs 2DEG Hall sensor, Sens. Actuators, A 102 (3) (2003) 216–222.
[17] ASTM: Standard Specification for Seamless Ferritic Alloy-Steel Pipe for High-Temperature Service, ASTM International, West Conshohocken, PA, 2009, a335/A335M-09a.
[18] ASTM: Standard Specification for Seamless Ferritic and Austenitic Alloy-Steel Boiler, Superheater, and Heat-Exchanger Tubes, ASTM International, West Conshohocken, PA, 2009, a213/A213M-09b.
[19] S. Saroja, M. Vijayalakshmi, V.S. Raghunathan, Effect of prolonged exposures of 9Cr–1Mo–0.07C steel to elevated temperatures, Mater. Trans 34 (10) (1993) 901–906.
[20] J.R. Yang, C.Y. Huang, C.N. Yang, J.L. Horng, Microstructural examination of 2.25Cr–1Mo steam pipes after extended service, Mater. Charact 30 (1993) 75–88.
[21] B. Arivazhagan, R. Prabhu, S. Albert, M. Kamaraj, S. Sundaresan, Microstructure and mechanical properties of 9Cr–1Mo steel weld fusion zones as a function of weld metal composition, J. Mater. Eng. Perform 18 (8) (2009) 999–1004.
[22] G. Sangdahl, M. Semchyshen, Application of 2.25Cr–1Mo Steel for Thick-Wall Pressure Vessels, ASTM International, Philadelphia, PA, 1982.
[23] C. Gatelier-Rothea, J. Chicos, R. Fougeres, P. Fleischmann, Characterization of pure iron and (130 p.p.m.) carbon–iron binary alloy by Barkhausen noise measurements: study of the influence of stress and microstructure, Acta Mater. 46 (14) (1998) 4873–4882.
[24] G. Bertotti, Hysteresis in Magnetism: for Physicists, Materials Scientists, and Engineers, Academic Press, San Diego, 1998.
[25] D.C. Jiles, A self consistent generalized model for the calculation of minor loop excursions in the theory of hysteresis, IEEE Trans. Magn. 28 (5) (1992) 2602–2604.
[26] J.W. Wilson, N. Karimian, W. Yin, J. Liu, M. Strangwood, C.L. Davis, A.J. Peyton Towards the development of a field deployable EM inspection tool for the evaluation of power station steels, in: Conference Proceedings of NDT 2013, Telford (2013).